JACS
JOURNAL OF THE AMERICAN CHEMICAL SOCIETY
Communication
pubs.acs.org/JACS

A Chlorin-Based Nanoscale Metal–Organic Framework for Photodynamic Therapy of Colon Cancers

Kuangda Lu,[†] Chunbai He,[†] and Wenbin Lin*

Department of Chemistry, University of Chicago, 929 East 57th Street, Chicago, Illinois 60637, United States

Supporting Information

ABSTRACT: We report here the rational design of the first chlorin-based nanoscale metal–organic framework (NMOF), DBC-UiO, with much improved photophysical properties over the previously reported porphyrin-based NMOF, DBP-UiO. Reduction of the DBP ligands in DBP-UiO to the DBC ligands in DBC-UiO led to a 13 nm red shift and an 11-fold increase in the extinction coefficient of the lowest-energy Q band. While inheriting the crystallinity, stability, porosity, and nanoplate morphology of DBP-UiO, DBC-UiO sensitizes more efficient $^1O_2$ generation and exhibits significantly enhanced photodynamic therapy (PDT) efficacy on two colon cancer mouse models as a result of its improved photophysical properties. Both apoptosis and immunogenic cell death contributed to killing of cancer cells in DBC-UiO-induced PDT.

Photodynamic therapy (PDT) combines three intrinsically nontoxic components—a photosensitizer (PS), light, and oxygen in target tissue—to generate cytotoxic reactive oxygen species (ROS), particularly singlet oxygen ($^1O_2$), to cause cell apoptosis and necrosis.[1] By localized delivery of the PS and light irradiation, PDT can minimize collateral damage to normal tissues in comparison with other systemic treatment modalities and, as a result, has been adopted to treat cancer and other diseases in recent years.[2]

Nanoparticles have been explored as an alternative to deliver PSs to tumors in order to enhance the PDT efficiency.[3] However, nanoparticle PSs have met limited success in PDT because of the difficulty in simultaneously optimizing ROS generation and transport to intracellular organelles to cause cell death. We recently reported the first successful use of a porphyrin-based nanoscale metal–organic framework (NMOF), DBP-UiO, as a PS for PDT.[4] DBP-UiO is stable in aqueous environments, and its 5,15-di(*p*-benzoato)porphyrin (DPB) ligands are well-separated from each other to avoid self-quenching. The coordination of heavy Hf^{4+} ions to the carboxylate groups of the DBP ligands enhances intersystem crossing (ISC) to increase the $^1O_2$ generation efficiency, while the nanoplate morphology and porous structure of DBP-UiO facilitate the diffusion of ROS out of the MOF interior, leading to highly effective PDT of resistant head and neck cancers. Despite the excellent performance in pilot animal studies, the photophysical properties of DBP-UiO are not optimal, with the lowest-energy absorption at 634 nm and a relatively small extinction coefficient (ε) of 2200 $M^{-1}\cdot cm^{-1}$. Herein we report the rational design of a chlorin-based NMOF, DBC-UiO (Scheme 1), with much improved photophysical properties and PDT efficacy in two colon cancer mouse models. It is worth noting that although numerous porphyrin-based MOFs have been reported in recent years,[5] DBC-UiO represents the first chlorin-based MOF.

Scheme 1. Schematic Description of Singlet Oxygen Generation by DBC-UiO Photosensitization with LED Light

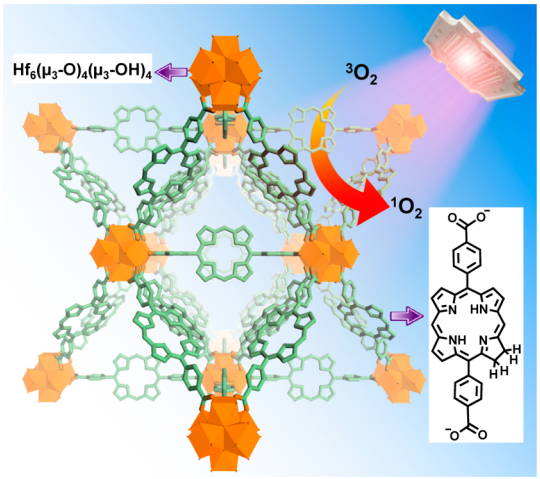

Hematoporphyrin derivatives were developed as the first generation of PSs, leading to the clinical application of the first PDT agent, photofrin, in 1993.[6] However, the photophysical properties of porphyrins are nonideal, with the absorption peaks typically near the high-energy edge of the tissue-penetrating window (600–900 nm) and small ε values. In molecular PS design, reduction of porphyrins to chlorins causes bathochromic shifts with a concomitant increase in ε.[7,8] For example, reduction of 5,10,15,20-tetra(*m*-hydroxyphenyl)porphyrin to its chlorin derivative shifts the last Q band from 644 to 650 nm and increases ε from 3400 to 29600 $M^{-1}\cdot cm^{-1}$. We hypothesized that a chlorin-based NMOF would have improved photophysical properties compared with DBP-UiO, leading to more effective PDT.

Partial reduction of 5,15-di(*p*-methylbenzoato)porphyrin (Me_2DBP) with toluenesulfonhydrazide yielded 5,15-di(*p*-methylbenzoato)chlorin (Me_2DBC) in 26% yield. Base-catalyzed hydrolysis of Me_2DBC afforded 5,15-di(*p*-benzoato)-chlorin (H_2DBC) in 88% yield. Me_2DBC and H_2DBC were

Received: April 20, 2015
Published: June 12, 2015

DOI: 10.1021/jacs.5b04069
J. Am. Chem. Soc. 2015, 137, 7600–7603

characterized by NMR spectroscopy and mass spectrometry (Figures S1−S4 in the Supporting Information [SI]). A solvothermal reaction between $HfCl_4$ and H_2DBC in *N*,*N*-dimethylformamide (DMF) afforded DBC-UiO as a dark-purple powder, which was washed with DMF, 1% (v/v) triethylamine (NEt_3) in ethanol, and ethanol in succession and then stored as a stock suspension in ethanol.

Powder X-ray diffraction (PXRD) indicated that DBC-UiO adopts the same UiO-type structure as DBP-UiO as a result of the geometric similarity between the DBC and DBP ligands (Figure 1a). The $Hf_6(\mu_3\text{-}O)_4(\mu_3\text{-}OH)_4$ secondary building units

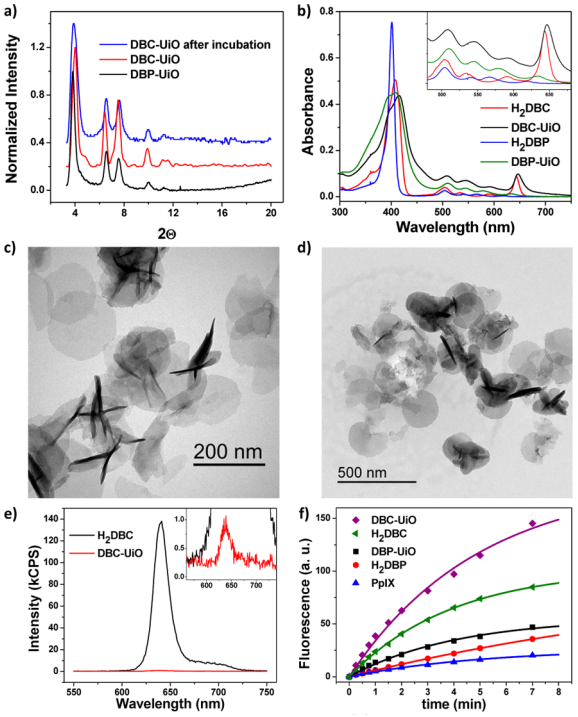

Figure 1. Characterization of DBC-UiO. (a) PXRD patterns of DBP-UiO and DBC-UiO before and after incubation in cell culture medium. (b) UV−vis absorption spectra of H_2DBC, DBC-UiO, H_2DBP, and DBP-UiO in DMF or 0.67 mM PBS. (c, d) TEM images of DBC-UiO showing nanoplate morphology (c) before and (d) after incubation in cell culture medium. (e) Steady-state fluorescence of 1 μM aqueous solutions of H_2DBC and DBC-UiO. (f) $^1O_2$ generation by DBC-UiO, H_2DBC, DBP-UiO, H_2DBP, and PpIX at an irradiance of 0.1 W/cm^2. DBC-UiO and H_2DBC were irradiated with a 650 nm LED, while the others were irradiated with a 640 nm LED. The symbols show experimental data, and the solid lines are fitted curves.

in DBC-UiO are connected by DBC ligands to afford a UiO framework of $Hf_6(\mu_3\text{-}O)_4(\mu_3\text{-}OH)_4(DBC)_6$. The Hf content was determined by inductively coupled plasma mass spectrometry (ICP-MS) to be 24.0% (calcd 23.8%), whereas a DBC weight loss of 64% (calcd 72%) was observed in thermogravimetric analysis (Figure S5).

Transmission electron microscopy (TEM) of DBC-UiO revealed a nanoplate morphology similar to that of DBP-UiO (Figure 1c). The plate diameters are 100−200 nm, while the thickness varies from 3.3 to 7.5 nm as determined by direct observation of particles lying perpendicular to the TEM grid (Figure S6). Notably, since the calculated distance between neighboring (111) packing layers (d_{111}) of the UiO structure is 2.2 nm, the ultrathin plates consist of only two to four sets of (111) packing layers. Such plates are even thinner than DBP-UiO plates (~10 nm in thickness), further facilitating ROS diffusion during PDT. Dynamic light scattering (DLS) measurements on DBC-UiO gave an average diameter of 128.5 nm with a polydispersity index of 0.17 and a ζ potential of −10.2 mV in phosphate-buffered saline (PBS) (Figure S7).

UV−vis absorption spectroscopy confirmed the improved photophysical properties of chlorin-based PSs (Figure 1b). H_2DBC has a split Soret band at λ_{max} = 408 nm and four Q bands at 504, 534, 591, and 643 nm. DBC-UiO shows slight red shifts for all of the Q bands relative to H_2DBC, with peaks at 508, 545, 592, and 646 nm. The lowest-energy Q band of DBC-UiO is thus red-shifted by 13 nm relative to DBP-UiO with an ε value of 24 600 M^{-1}·cm^{-1}, which is 11-fold greater than that of DBP-UiO. H_2DBC has an ε value of 21 800 M^{-1}·cm^{-1} for the lowest-energy Q band, which is 13-fold greater than that of H_2DBP (1700 M^{-1}·cm^{-1}).

H_2DBC exhibits a fluorescence peak at ~641 nm (Figure 1e), but the DBC-UiO fluorescence is ~200-fold weaker than that of H_2DBC because of enhanced ISC upon coordination of the DBC ligands to Hf^{4+} ions via the carboxylate groups. DBC-UiO has a slightly shorter fluorescence lifetime of 7.88 ns compared with H_2DBC (8.15 ns) as determined by time-correlated single-photon counting measurements (Figure S10 and Table S1 in the SI).

Singlet Oxygen Sensor Green (SOSG) was employed to determine the $^1O_2$ generation efficiencies of H_2DBC and DBC-UiO. SOSG reacts with generated $^1O_2$ to give green fluorescence (λ_{em} = 525 nm) that can be quantified with a fluorimeter. For comparison, the $^1O_2$ generation efficiencies of H_2DBP, DBP-UiO, and protoporphyrin IX (PpIX) were also determined. The plot of fluorescence intensity (I_F) against irradiation time (t) was fitted with an exponential function (eq 1):

$$I_F = A(1 - e^{-kt}) \quad (1)$$

where A and k are fitting parameters (Table 1).[4] The fits, which are shown in Figure 1f, indicate a pseudo-first-order $^1O_2$ generation process.[4] The total $^1O_2$ generation yields were normalized to that of PpIX to allow a comparison of the overall photosensitization efficiencies. DBC-UiO is ~3 times as efficient as DBP-UiO in generating $^1O_2$.

Table 1. Fitting Parameters for $^1O_2$ Generation Curves

	A	k (min^{-1})	normalized yield
H_2DBC	102	0.25	4.3
DBC-UiO	195	0.18	7.3
H_2DBP	101	0.06	1.8
DBP-UiO	55.9	0.24	2.4
PpIX	26.6	0.19	1

The stability of DBC-UiO in biological media was confirmed by TEM and PXRD after culturing the NMOF in RPMI 1640 cell culture medium for 12 h. The morphology of NMOFs did not change, as shown by TEM (Figure 1d), while high-resolution TEM images along with their fast Fourier transform patterns indicated retention of the NMOF crystallinity (Figure S11). The PXRD pattern of DBC-UiO did not change after incubation in RPMI 1640 cell culture medium (Figure 1a), further proving the framework stability of DBC-UiO in biological environments.

DBC-UiO not only retains all of the attributes of DBP-UiO (a crystalline and stable structure to avoid self-quenching even at 64% PS loading, enhanced ISC to increase the $^1O_2$ generation efficiency, and a porous framework and nanoplate morphology to

DOI: 10.1021/jacs.5b04069
J. Am. Chem. Soc. 2015, 137, 7600−7603

facilitate $^1O_2$ diffusion) but also possesses significantly enhanced photophysical properties. We tested the PDT efficacy of DBC-UiO against murine and human colorectal cancers. PDT is used in the clinic to treat colon cancer by delivering light through an endoscope.[9] It is also known that PDT treatment of primary colon tumors can elicit immunogenic response on metastatic tumors.[10]

The tumor cell uptakes of the NMOFs were evaluated by incubating CT26 cells with DBP-UiO or DBC-UiO at a Hf^{4+} concentration of 50 μM for 4 h. The Hf contents in CT26 cells were determined by ICP-MS to be (34.4 ± 1.3) and (23.5 ± 0.8) nmol/10^6 cells for DBP-UiO and DBC-UiO, respectively. The cellular uptakes of DBC-UiO and H_2DBC by CT26 and HT29 in terms of ligand concentrations were also determined by UV−vis analysis (Figures S12 and S13). The in vitro PDT efficacies of DBC-UiO against colon cancer cells were investigated and compared with those of DBP-UiO and the corresponding free ligands. NMOFs or free ligands were incubated with CT26 or HT29 cells at various concentrations, and the cells were irradiated with light from a light-emitting diode (LED) (DBP-UiO and H_2DBP, 640 nm; DBC-UiO and H_2DBP, 650 nm) at a total light dose of 90 J/cm^2 (0.1 W/cm^2 for 15 min). DBC-UiO outperformed DBP-UiO by effectively killing both cancer cell lines at low NMOF and light doses (Figure 2a,b). Groups treated with free ligand also showed moderate PDT efficacy, while no cytotoxicity was observed in dark or PBS control groups. The IC_{50} values for DBC-UiO, H_2DBC, DBP-UiO, and H_2DBP in CT26 cells with irradiation were calculated to be 5.1 ± 0.2, 8.5 ± 0.1, 10.4 ± 0.5, and 20.0 ± 3.1 μM, respectively, and those in HT29 cells with irradiation were calculated to be 6.0 ± 1.5, 7.5 ± 2.3, 13.1 ± 2.2, and 17.0 ± 4.0 μM, respectively. These results confirm that DBC-UiO is a more potent PS than DBP-UiO in PDT as a result of the enhanced photophysical properties. DBC-UiO showed PDT cytotoxicity in murine macrophage Raw264.7 cells, but a higher ligand concentration (>20 μM) was required to achieve 50% cell killing (Figure S14).

We further showed that both apoptosis and immunogenic cell death (ICD) contribute to the superior in vitro PDT efficacy. CT26 cells were incubated with 5 μM DBC-UiO or H_2DBC followed by light irradiation at 0.1 W/cm^2 for 15 min (90 J/cm^2). The apoptosis induced by PDT treatment was determined by flow cytometry using an Alexa Fluor 488 Annexin V/dead cell apoptosis kit. No apoptosis or necrosis was observed for cells treated with DBC-UiO or H_2DBC in the dark, while significant numbers of cells underwent apoptosis when treated with DBC-UiO or H_2DBC upon light irradiation (Figures 2c and S15). Calreticulin (CRT) is a distinct biomarker exposed on the surface of cells undergoing ICD.[11] The CRT expression was determined by flow cytometry and immunofluorescence to assess the ICD induced by DBC-UiO-induced PDT. CT26 cells were treated with 5 μM DBC-UiO or H_2DBC followed by light irradiation at 0.1 W/cm^2 for 15 min (90 J/cm^2). For flow cytometry analysis, cells were collected and stained with Alexa Fluor 488−CRT antibody and propidium iodide (PI) (Figures 2d and S16). The fluorescence intensity of stained cells was gated on PI-negative cells. For immunostaining analysis, the cells were stained with AlexaFluor 488−CRT and DAPI and observed using confocal laser scanning microscopy (CLSM) (Figures 2e and S17). Cells treated with DBC-UiO or H_2DBC without light irradiation showed no surface CRT expression, while significant amounts of CRT were detected on the surface of cells upon irradiation. These results indicate that ICD was involved in the cytotoxicity induced by PDT of DBC-UiO and H_2DBC.

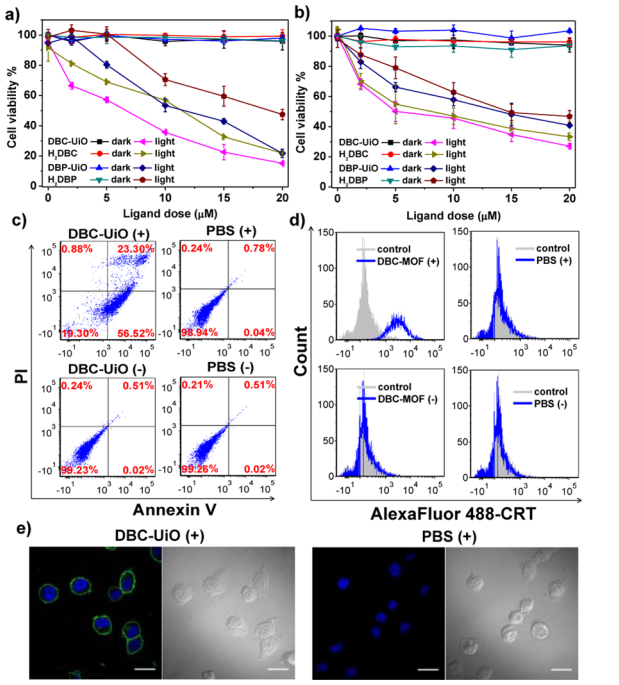

Figure 2. In vitro PDT efficacy and mechanisms of action. (a, b) PDT cytotoxicities of DBC-UiO, DBP-UiO, H_2DBC, and H_2DBP at different PS concentrations in (a) CT26 and (b) HT29 cells. (c) Annexin V/PI analysis of CT26 cells incubated with DBC-UiO or PBS with (+) or without (−) light irradiation (90 J/cm^2). The quadrants from lower left to upper left (counterclockwise) represent healthy, early apoptotic, late apoptotic, and necrotic cells, respectively. The percentages of cells in each quadrant are shown on the graphs. (d) CRT exposure on the cell surface of CT26 cells was assessed by flow cytometry analysis after incubation with DBC-UiO or PBS with or without irradiation (90 J/cm^2). The fluorescence intensity was gated on PI-negative cells. (e) Immunofluorescence microscopy of CRT expression on the cell surface of CT26 cells treated with DBC-UiO or PBS upon irradiation (90 J/cm^2). Blue: DAPI-stained nuclei. Green: Alexa Fluor 488−CRT antibody. Scale bars = 20 μm.

We carried out in vivo anticancer efficacy experiments on subcutaneous flank tumor mouse models of CT26 and HT29. The mice were intratumorally injected with (1) PBS control, (2) DBC-UiO, (3) DBP-UiO, (4) H_2DBC, or (5) H_2DBP at a ligand dose of 1 mg/kg or (6) DBC-UiO at a ligand dose of 3.5 mg/kg. Twelve hours post injection, each mouse in groups 1−5 was irradiated at the tumor site with light (0.1 W/cm^2) for 15 min (90 J/cm^2), and the mice in group 6 received light irradiation (0.1 W/cm^2) for 30 min (180 J/cm^2). For groups 1−5 on the CT26 model, mice were treated again 4 days after the first treatment, while for groups 1−5 on the HT29 model, mice were treated every 4 days for a total of four treatments. As depicted in Figure 3a,c, the tumor growth of mice treated with DBC-UiO (1 mg/kg DBC dose) was effectively inhibited in both models. DBP-UiO and the two PS ligands failed to suppress the tumor growth in either model because of low PS and light doses. Higher doses of DBC-UiO and light irradiation led to effective tumor regression in HT29 with a single treatment and in CT26 with two treatments (Figure 3a,c). The weights and sizes of tumors treated with DBC-UiO at the end point were also significantly smaller than for the other groups (Figures 3b and S20 for the CT26 model; Figures 3d and S21 for the HT29 model; Table S2). Histology of frozen tumor slices further confirmed that only DBC-UiO treatment caused apoptosis/necrosis of tumors, while

DOI: 10.1021/jacs.5b04069
J. Am. Chem. Soc. 2015, 137, 7600−7603

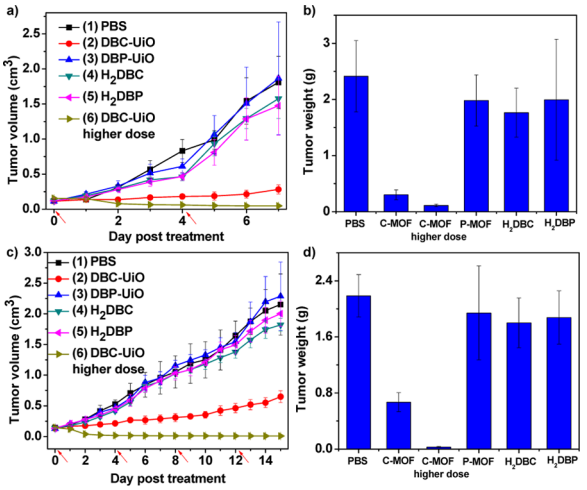

Figure 3. In vivo PDT efficacy on CT26 and HT29 tumor-bearing mice. (a, c) Tumor growth inhibition curves after PDT treatment in the (a) CT26 and (c) HT29 models. Red arrows refer to treatment time points (for group 6 in the HT29 model, only one treatment was received). (b, d) Tumor weights after PDT treatment in the (b) CT26 and (d) HT29 models.

treatment with DBP-UiO or the two PS ligands did not (Figure S22). Along with the in vitro PDT results, the superior anticancer efficacies achieved by DBC-UiO in both colorectal cancer models indicate that DBC-UiO is a more efficient photosensitizer than DBP-UiO.

In summary, we have rationally designed the first chlorin-based NMOF, DBC-UiO, with exceptionally high PS loading, crystallinity, framework stability, porosity, nanoplate morphology, and enhanced intersystem crossing. Importantly, DBC-UiO exhibits a 13 nm red shift and an 11-fold increase in the extinction coefficient of the lowest-energy Q band relative to the previously reported DBP-UiO. As a result, DBC-UiO is 3 times as efficient as DBP-UiO in generating $^1O_2$ and exhibits much higher PDT cytotoxicity in two colon cancer cell lines. The superior anticancer efficacy of DBC-UiO compared with DBP-UiO was also demonstrated in two colorectal adenocarcinoma mouse models. We further elucidated that both apoptosis and immunogenic cell death contribute to cell killing induced by DBC-UiO-based PDT. NMOFs thus provide an excellent platform for achieving highly efficient PDT via both apoptosis and ICD and represent a novel class of nanomedicine with significant potential for clinical translation.[12]

■ ASSOCIATED CONTENT

Ⓢ Supporting Information

Synthesis and characterization of H_2DBP and DBP-UiO and cellular uptake and in vitro and in vivo efficacy studies. The Supporting Information is available free of charge on the ACS Publications website at DOI: 10.1021/jacs.5b04069.

■ AUTHOR INFORMATION

Corresponding Author

*wenbinlin@uchicago.edu

Author Contributions

†K.L. and C.H. contributed equally.

Notes

The authors declare no competing financial interest.

■ ACKNOWLEDGMENTS

We thank NIH (UO1-CA151455) for funding support and Dr. Cheng Wang, Teng Zhang, Zekai Lin, Christopher Poon, and Dr. Carter Abney for experimental help. We acknowledge the use of the University of Chicago Biophysical Dynamics NanoBiology Facility (NIH Grant 1S10RR026988-01) and facilities of the University of Chicago Medicine Comprehensive Cancer Center (NIH CCSG P30 CA014599).

■ REFERENCES

(1) (a) Pass, H. I. *J. Natl. Cancer Inst.* **1993**, *85*, 443. (b) Celli, J. P.; Spring, B. Q.; Rizvi, I.; Evans, C. L.; Samkoe, K. S.; Verma, S.; Pogue, B. W.; Hasan, T. *Chem. Rev.* **2010**, *110*, 2795.

(2) (a) Allison, R. R.; Sibata, C. H. *Photodiagn. Photodyn. Ther.* **2010**, *7*, 61. (b) Agostinis, P.; Berg, K.; Cengel, K. A.; Foster, T. H.; Girotti, A. W.; Gollnick, S. O.; Hahn, S. M.; Hamblin, M. R.; Juzeniene, A.; Kessel, D. *CA-Cancer J. Clin.* **2011**, *61*, 250.

(3) (a) Roy, I.; Ohulchanskyy, T. Y.; Pudavar, H. E.; Bergey, E. J.; Oseroff, A. R.; Morgan, J.; Dougherty, T. J.; Prasad, P. N. *J. Am. Chem. Soc.* **2003**, *125*, 7860. (b) Chatterjee, D. K.; Fong, L. S.; Zhang, Y. *Adv. Drug Delivery Rev.* **2008**, *60*, 1627. (c) Cheng, Y.; Samia, A. C.; Meyers, J. D.; Panagopoulos, I.; Fei, B.; Burda, C. *J. Am. Chem. Soc.* **2008**, *130*, 10643. (d) Jin, C. S.; Cui, L.; Wang, F.; Chen, J.; Zheng, G. *Adv. Healthcare Mater.* **2014**, 3, 1240. (e) Lovell, J. F.; Jin, C. S.; Huynh, E.; Jin, H.; Kim, C.; Rubinstein, J. L.; Chan, W. C.; Cao, W.; Wang, L. V.; Zheng, G. *Nat. Mater.* **2011**, *10*, 324. (f) Idris, N. M.; Gnanasammandhan, M. K.; Zhang, J.; Ho, P. C.; Mahendran, R.; Zhang, Y. *Nat. Med.* **2012**, *18*, 1580. (g) Juzenas, P.; Chen, W.; Sun, Y.-P.; Coelho, M. A. N.; Generalov, R.; Generalova, N.; Christensen, I. L. *Adv. Drug Delivery Rev.* **2008**, *60*, 1600. (h) Carter, K. A.; Shao, S.; Hoopes, M. I.; Luo, D.; Ahsan, B.; Grigoryants, V. M.; Song, W.; Huang, H.; Zhang, G.; Pandey, R. K.; Geng, J.; Pfeifer, B. A.; Scholes, C. P.; Ortega, J.; Karttunen, M.; Lovell, J. F. *Nat. Commun.* **2014**, *5*, No. 3546. (i) Cheng, L.; Wang, C.; Feng, L.; Yang, K.; Liu, Z. *Chem. Rev.* **2014**, *114*, 10869.

(4) Lu, K.; He, C.; Lin, W. *J. Am. Chem. Soc.* **2014**, *136*, 16712.

(5) (a) Kosal, M. E.; Chou, J.-H.; Wilson, S. R.; Suslick, K. S. *Nat. Mater.* **2002**, *1*, 118. (b) Fateeva, A.; Chater, P. A.; Ireland, C. P.; Tahir, A. A.; Khimyak, Y. Z.; Wiper, P. V.; Darwent, J. R.; Rosseinsky, M. J. *Angew. Chem.* **2012**, *124*, 7558. (c) Zhang, Z.; Zhang, L.; Wojtas, L.; Nugent, P.; Eddaoudi, M.; Zaworotko, M. J. *J. Am. Chem. Soc.* **2012**, *134*, 924. (d) Farha, O. K.; Shultz, A. M.; Sarjeant, A. A.; Nguyen, S. T.; Hupp, J. T. *J. Am. Chem. Soc.* **2011**, *133*, 5652. (e) Wang, X.-S.; Meng, L.; Cheng, Q.; Kim, C.; Wojtas, L.; Chrzanowski, M.; Chen, Y.-S.; Zhang, X. P.; Ma, S. *J. Am. Chem. Soc.* **2011**, *133*, 16322. (f) Feng, D.; Gu, Z. Y.; Li, J. R.; Jiang, H. L.; Wei, Z.; Zhou, H. C. *Angew. Chem.* **2012**, *124*, 10453. (g) Johnson, J. A.; Zhang, X.; Reeson, T. C.; Chen, Y.-S.; Zhang, J. *J. Am. Chem. Soc.* **2014**, *136*, 15881. (h) DeVries, L. D.; Barron, P. M.; Hurley, E. P.; Hu, C.; Choe, W. *J. Am. Chem. Soc.* **2011**, *133*, 14848. (i) Zou, C.; Zhang, Z.; Xu, X.; Gong, Q.; Li, J.; Wu, C.-D. *J. Am. Chem. Soc.* **2012**, *134*, 87. (j) Yang, X.-L.; Xie, M.-H.; Zou, C.; He, Y.; Chen, B.; O'Keeffe, M.; Wu, C.-D. *J. Am. Chem. Soc.* **2012**, *134*, 10638.

(6) Dougherty, T. J. *Photochem. Photobiol.* **1993**, *58*, 895.

(7) Ash, D.; Brown, S. *Eur. J. Cancer* **1993**, *29*, 1781.

(8) Senge, M. O.; Brandt, J. C. *Photochem. Photobiol.* **2011**, *87*, 1240.

(9) (a) Gahlen, J.; Prosst, R. L.; Stern, J. *Chirurg* **2002**, *73*, 122. (b) Mlkvy, P.; Majek, F.; Jurgos, L.; Makovnik, P.; Durdik, S. *Bratislava Med. J.* **2010**, *111*, 50.

(10) (a) Garg, A. D.; Agostinis, P. *Photochem. Photobiol. Sci.* **2014**, *13*, 474. (b) Galluzzi, L.; Kepp, O.; Kroemer, G. *EMBO J.* **2012**, *31*, 1055. (c) Tanaka, M.; Kataoka, H.; Takashi, J. *Dig. Dis. Sci.* **2014**, *59*, 2018.

(11) Kroemer, G.; Galluzzi, L.; Kepp, O.; Zitvogel, L. *Annu. Rev. Immunol.* **2013**, *31*, 51.

(12) (a) Della Rocca, J.; Liu, D.; Lin, W. *Acc. Chem. Res.* **2011**, *44*, 957. (b) He, C.; Lu, K.; Lin, W. *J. Am. Chem. Soc.* **2014**, *136*, 5181.

DOI: 10.1021/jacs.5b04069
J. Am. Chem. Soc. 2015, 137, 7600−7603